Bioelectrochemistry 132 (2020) 107440

Contents lists available at ScienceDirect

Bioelectrochemistry

journal homepage: www.elsevier.com/locate/bioelechem

Contactless electroporation induced by high intensity pulsed electromagnetic fields via distributed nanoelectrodes

Damijan Miklavcic [a,*], Vitalij Novickij [b], Matej Kranjc [a], Tamara Polajzer [a], Sasa Haberl Meglic [a], Tina Batista Napotnik [a], Rok Romih [c], Darja Lisjak [d]

[a] University of Ljubljana, Faculty of Electrical Engineering, Trzaska 25, SI-1000 Ljubljana, Slovenia
[b] Institute of High Magnetic Fields, Vilnius Gediminas Technical University, Naugarduko g. 41, 03227 Vilnius, Lithuania
[c] University of Ljubljana, Faculty of Medicine, Institute of Cell Biology, Vrazov trg 2, SI-1000 Ljubljana, Slovenia
[d] Jozef Stefan Institute, Department for Materials Synthesis, Jamova cesta 39, SI-1000 Ljubljana, Slovenia

ARTICLE INFO

Article history:
Received 26 September 2019
Received in revised form 3 December 2019
Accepted 5 December 2019
Available online 13 December 2019

Keywords:
Magnetic fields
Membrane permeabilization
Gold nanoparticles
Propidium iodide
Yo-pro-1
Non-invasive electroporation
Distributed nanoelectrodes

ABSTRACT

Pulsed electric fields (PEFs) can be used to transiently increase cell membrane permeability in procedures ranging from gene therapy to tumor eradication. Although very efficient, PEF-based therapies generally require the use of invasive electrodes, which cause pain and tissue damage. An emerging noninvasive, contactless alternative to PEFs are High Intensity Pulsed Electromagnetic Fields (HI-PEMF), whereby the electric field inside the tissue is induced remotely by external pulsed magnetic field. However, one of the current major drawbacks of HI-PEMFs is their inferior efficiency compared to PEFs. In this study we present the proof-of-concept that by adding highly conductive 5 and 20 nm gold nanoparticles (Au NPs), we can significantly potentiate the permeabilizing effect of HI-PEMFs, making it possible to permeabilize up to 80% of the cells with minimal or no effect on cell survival, compared to negligible percentage of permeabilized cells using HI-PEMF alone. Experiments, conducted on Chinese Hamster Ovary cells and *Escherichia coli*, suggest that Au NPs act as distributed nanoelectrodes, locally enhancing the electric field induced at the plasma membrane. Our findings open up an avenue of possibilities for combining naked as well as functionalized Au NPs with HI-PEMFs for noninvasive, remotely controlled smart drug delivery applications.

1. Introduction

Pulsed electric field (PEF) treatment is becoming a promising technique for permeabilization of cell membrane. The technique is also known as electroporation and has gained considerable attention in the last few decades. The technique is based on a phenomenon characterized by transient increase of cell membrane permeability to molecules, which otherwise have poor or no transmembrane transport mechanisms, by exposure of cells to externally applied pulsed electric fields [1–4]. Electroporation was demonstrated in eukaryotes, prokaryotes and archaea as well as in artificial membranes [5–8]. All conventional electroporation applications require direct contact between the electrodes and the treated object, that is, either via plate electrodes which embrace the tissue, or using invasive needle electrodes, which are inserted into the tissue. The use of invasive electrodes, such as needle electrodes which are most effective in electroporation treatment of a variety of tissues have a number of drawbacks common to all invasive procedures, e.g., assuring sterile incisions and causing trauma to tissues by incision. There are additional side effects due to application of electric pulses, such as the dependence of electric field distribution on the dielectric properties of the sample [9–12], presence of electrochemical reactions in the electrode-electrolyte/tissue interfaces [13], extreme changes of pH [14,15] and the possibility of electrical breakdown between the electrodes [16,17].

Recently, we demonstrated that membrane permeabilization *in vitro* and *in vivo* can be achieved also by High Intensity Pulsed Electromagnetic Fields (HI-PEMF) [18,19], *i.e.*, by inducing electric field in the treated sample without physical contact using time varying magnetic field [18–20]. We stipulated that the phenomena underlying observed permeabilization *in vitro* and enhanced accumulation of platinum in cells and chemotherapeutic effect in murine tumor model is membrane electroporation [19].

* Corresponding author at: University of Ljubljana, Faculty of Electrical Engineering, Trzaska 25, SI-1000 Ljubljana, Slovenia.
E-mail address: Damijan.Miklavcic@fe.uni-lj.si (D. Miklavcic).

https://doi.org/10.1016/j.bioelechem.2019.107440
1567-5394/

Electroporation remains the working hypothesis in spite of the fact that induced electric fields as calculated/estimated are in the order of 1 V/cm, which is 100–1000 times lower from what is assumed to be reversible threshold electric field for membrane permeabilization *in vitro* [21–24] and *in vivo* [25–27] when using conventional electroporation by means of PEF. Nevertheless, the increase of the induced electric field component during HI-PEMF treatment results in higher permeabilization of cells [18,20,28].

In this study, we decided to enhance the induced electric field locally, *i.e.*, close to the membrane, by means of distributed nanoelectrodes in the form of highly conductive gold nanoparticles (Au NPs). It has been namely theoretically predicted that presence of conductive NPs close to the membrane during PEF treatment results in local enhancement of electric field [29–32], thus leading to membrane electroporation at lower electric fields [33]. Improvement of PEF treatment by addition of Au NPs was already observed experimentally *in vitro* by showing increased mammalian cells transfection [34,35] and efficiency in anticancer therapy [33,36].

The aim of our present work was to study the feasibility of enhancing the effect of HI-PEMF by enabling higher efficacy of contactless membrane permeabilization through distributed nanoelectrodes in the form of Au NPs. As a proof of concept, the study was performed by application of HI-PEMF on eukaryotic and prokaryotic cells with two different sizes of Au NPs. The Au NPs mediated membrane electroporation by means of HI-PEMF was determined by the membrane permeabilization and survival assays. For comparison, conventional electroporation by means of PEF was used as a reference.

2. Material and methods

2.1. Gold nanoparticles

All gold nanoparticles (Au NPs) used in this study were obtained from Sigma-Aldrich. Au NPs size 5 nm (cat. no. 741949), 20 nm (cat. no. 741965) in citrate buffer, and 20 nm (cat. no 753610) in PBS buffer were diluted with KPB electroporation buffer (for CHO cells) or distilled water (for bacteria) to get various concentrations of nanoparticles: 50, 25 and 10 μg/ml. The particle morphologies and sizes were characterized with a transmission electron microscope Jeol 2100 (Jeol, Tokyo, Japan). The equivalent diameters of the particles were determined from their surfaces using Digital Micrograph Software (Gatan, Inc., Pleasanton, USA). A minimum of 250 particles per sample was counted for the statistics. The zeta-potential and hydrodynamic particle size of the as-received suspensions were obtained with Zeta Potential Analyzer equipped with Particle Sizer (Zetaplus, Brookhaven Instruments, Long Island, New York, USA). The pH (for measurements of the zeta-potential versus pH dependence) was adjusted with differently concentrated (0.01, 0.1 or 1 M) HCl or NaOH solutions.

2.2. High intensity pulsed electromagnetic fields and pulsed electric fields

For HI-PEMF generation the 550 A, 2 kV generator (Fig. 1A) has been used with a total 1.2 J accumulated energy of the pulse [20] in accordance with methodology developed in our previous work [18]. The magnetic field inductor, which served as a load of the system consisted of 11 windings and 6 layers (total of 66 windings) with a resulting total inductance of 9.8 μH. The inner diameter of the inductor was 3 mm to match the 0.1 ml PCR (Polymerase chain reaction) tube (STARLAB International GmbH, Hamburg, Germany). The duration of one HI-PEMF pulse was 15 μs and maximum amplitude was 5.5 T. The waveform of the pulse is shown in Fig. 1B.

The maximum induced electric field is proportional to the *dB/dt* of the pulse and was in the range of 8 V/cm [18]. Bursts of 50 pulses at low frequency (1 Hz) were used and a 30-second pause was introduced to allow cooling of the sample. The total number of pulses was 200 (50 × 4) with a total treatment time of 4 min 50 s. The temperature of the cell suspension did not exceed 36 °C throughout the whole treatment [18].

For PEF treatment of CHO cells, prototype H-bridge-based pulse generator made at University of Ljubljana, Faculty of Electrical Engineering was used [21]. The pulses were generated between stainless steel 304 plate electrodes (d = 2 mm) and a sequence of 8 × 100 μs square wave pulses of 0–1000 V was used in the study. For PEF treatment of *E. coli*, a square wave electric pulse generator HVP-VG (IGEA s.r.l., Carpi, Modena, Italy) was used. The pulses were generated between stainless steel 304 plate electrodes, rectangle shaped (d = 1 mm) and a sequence of 8 × 100 μs square wave pulses of 650 V was applied. Voltage and current waveforms of PEF setups are available in Supplementary Material (Fig. S3.)

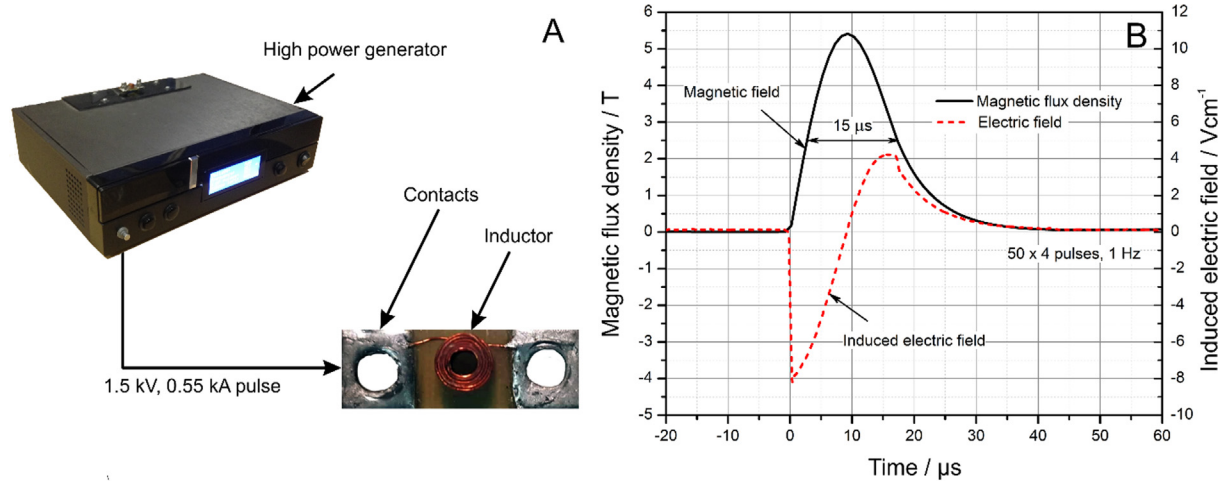

Fig. 1. Generation of HI-PEMF, where A – setup for *in vitro* experiments consisted of high power generator capable of generating up to 550 A, 2 kV pulses to inductor with 66 windings, B – The waveform of the applied magnetic field pulse (solid black line) and corresponding induced electric field pulse (dotted red line).

2.3. Cell permeabilization

Before cells were exposed to HI-PEMF treatment or PEF treatment, CHO cell suspension with or without Au NPs was mixed with fluorescent markers – either propidium iodide (PI) or YO-PRO®-1 (YP) (both Life Technologies, California, USA), to obtain a final concentration of 136 μM for PI, and 1 μM for YP. For HI-PEMF treatment the volume of the sample was limited to 20 μl (effective volume of the inductor), while in conventional electroporation 50 μl samples were put between the electrodes, but after pulse application only 40 μl was used. After the HI-PEMF and PEF treatment samples were incubated at room temperature (22 °C) for 3 min in order for fluorescent dye to enter permeabilized cells. Untreated samples were not exposed to any pulse treatment, but they were incubated at room temperature for the same time as treated samples. Cells were then diluted in 100 μl of KPB buffer to stop inflow of fluorescent dye and analyzed by fluorescent microscopy or flow cytometric analysis. For each parameter three repetitions in random order were done. The percentage of permeabilization was defined by gating of flow cytometer.

To evaluate permeabilization of *E. coli* cells, immediately before exposing cells to pulses PI was added, to obtain a final concentration of 136 μM for PI. HI-PEMF treatment was repeated 3-times (each time with a new sample) in order to obtain sufficiently large volume for further analysis. For electroporation 70 μl of *E. coli* cells were placed between electrodes and exposed to electric pulses. Control samples were not exposed to pulses (PEF or HI-PEMF). After the treatment samples were incubated in darkness at room temperature (22 °C) for 20 min in order for PI to enter permeabilized cells. *E. coli* cells were then centrifuged (16,099*g*, 5 min, 10 °C) to remove extracellular PI and pellet was re-suspended in distilled water. The uptake of PI was evaluated with spectrofluorometer Tecan (Tecan Infinite M200, Tecan, Grödig, Austria) at 617 nm. The percentage of permeabilization of *E. coli* cells was defined as:

$$\text{Permeabilization}(\%) = \frac{FL(E) - FL(E=0)}{FL(\max) - FL(E=0)} \quad (1)$$

where *FL(E)* symbolize fluorescence intensity of treated cells, *FL (E = 0)* fluorescence intensity of non-treated cells (cells in control) and *FL(*max*)* fluorescence intensity where saturation fluorescence is attained (8 × 100 μs, 19 kV/cm, 1 Hz).

2.4. CHO cells

Chinese hamster ovary cells (European Collection of Authenticated Cell Cultures ECACC, cells CHO-K1, cat. no. 85051005, obtained directly from the repository) were grown in culture flasks (TRP, Trasadingen, Switzerland) with growth medium for 2–3 days at 37 °C in a humidified 5% CO_2 atmosphere in the incubator (Kambič, Semič, Slovenia). Growth medium, HAM F-12, (PAA, Pasching, Austria) was supplemented with 10% fetal bovine serum (Sigma-Aldrich, Chemie GmbH, Deisenhofen, Germany), L-glutamine (StemCell, Vancouver, Canada) and antibiotics penicillin/streptomycin (PAA, Pasching, Austria), gentamycin (Sigma-Aldrich). On the day of experiment cells were detached by 10× trypsin-EDTA (PAA), diluted 1:9 in Hank's basal salt solution (StemCell). After 2 min trypsin was inactivated by addition of HAM F-12 growth medium to cell suspension. Cells were transferred to a 50 ml centrifuge tube (TRP) and centrifuged at 180 g and 22 °C for 5 min. Supernatant was removed and cells were mixed with only potassium phosphate electroporation buffer (KPB: 10 mM KH_2PO_4/K_2HPO_4 in a ratio of 40.5:9.5, 1 mM MgCl2, and 250 mM sucrose) or with different concentrations of Au NPs (Sigma-Aldrich) at cell density 2 × 10^6 cells/ml. Before the start of the experiment cells with added nanoparticles were incubated for either 0, 15, 30 or 60 min at 4 °C, though cells without added Au NPs was used immediately.

2.5. Bacterial cells

Escherichia coli K12 TOP10 with pEGFP-N1 (Clontech Laboratories Inc., Mountain View, CA, USA) coding kanamycin resistance was used. Bacterial cells were grown in Luria Broth liquid medium (Sigma-Aldrich) supplemented with 50 μg/ml of antibiotic kanamycin sulphate (Carl ROTH Gmbh, Essen, Germany). Bacterial cells were agitated at 37 °C to early exponential growth phase, collected by centrifugation (4248*g*, 30 min, 4 °C) and re-suspended in distilled water to attain approximately 1.6 × 10^9 CFU/ml. Bacteria were again centrifuged (9055*g*, 5 min, 10 °C), supernatant was removed and *E. coli* cells were mixed at cell density of 7 × 10^8 CFU/ml with 50 μg/ml of 5 and 20 nm gold nanoparticles (Sigma-Aldrich) in distilled water or only with distilled water. *E. coli* cells were incubated with Au NPs for 1 h at 4 °C before the treatment.

2.6. Flow cytometry

Three minutes after the last pulse, CHO cell suspension was transferred to 1.5 ml tube (BRAND GMBH + CO KG, Germany), mixed with 130 μl KPB and analyzed by flow cytometer (Attune NxT; Life Technologies, Carlsbad, CA, USA). For detection of PI fluorescence, samples were excited with a blue laser at 488 nm and the emitted fluorescence was detected through a 574/26 nm band-pass filter. For YP we used the same laser but different (530/30 nm) band-pass filter. The measurement was stopped when 10,000 events was obtained. For data analysis, Attune Nxt software was used. On the dot plot of forward-scatter versus side-scatter cells were separated from debris. Aggregates of cells were removed from analysis in dot plot of forward-scatter – area versus forward-scatter – height. This way only single cells were considered in analysis. Histogram of fluorescence intensity was used for determining fluorescence in two ways. First was the fluorescence of median value of the measured signal from cells. Each parameter was calculated by normalizing to control sample. Second was the number of fluorescent cells, which was determined by additional gating. Gate for PI and YP fluorescent cells was set with the use of negative control (no treatment applied) and positive control (PEF treated; 1.5 kV/cm, square pulses 8 × 100 μs).

2.7. Fluorescence microscopy

Three minutes after HI-PEMF or PEF treatment, CHO cell suspension was diluted in 40 μl of KPB buffer and transferred to 96-well plate. Bright-field and fluorescence images were acquired using an inverted microscope AxioVert 200 (Zeiss, Oberkochen, Germany) with 20× or 40× objectives, with excitation light 510 nm for PI and 491 nm for YP, using a polychromatic illumination system (Visitron Systems GmbH, Puchheim, Germany) and appropriate filter sets: with emission 605/54 nm for PI and 535/30 nm for YP (filter sets 71,006 and 41,028, respectively; Chroma Technology Corp., Bellows Falls, VT, USA). Images were acquired using VisiCam 1280 CCD camera (Visitron Systems GmbH, Puchheim, Germany) and the MetaMorph PC software for image acquisition (Molecular Devices, Sunnyvale, CA, USA). Light exposure times were 1 s for PI and 1 and 10 s for YP (due to low

fluorescence of YP). Obtained pictures were analyzed using ImageJ (National Institutes of Health, Bethesda, MD, USA).

2.8. Cell survival

CHO cell survival was assessed via metabolic activity MTS assay (CellTiter 96® AQueous One Solution Cell Proliferation Assay (MTS), Promega, Wisconsin, USA), according to the manufacturers protocol. First the impact of Au NPs on cell survival without any pulse treatment were investigated. Cells were mixed with 50 μg/μl of 5 and 20 nm Au NPs for citrate buffer and 20 nm Au NPs form PBS buffer or only with KPB buffer

When testing the effect of PEF on survival of cells with different Au NPs, 50 μl of cell suspension was placed between the electrodes. The effect of HI-PEMF was tested on cell suspension with 50 μg/μl of 20 nm Au NPs. HI-PEMF treated and untreated samples were used. The following steps were the same for all survival assays. After pulse application samples were transferred in HAM F-12 growth media and 100 μl was plated in a 96-well plate (TPP). Plate was then transferred in the incubator at 37 °C and humidified 5% CO2 atmosphere. After 24 h 20 μl of MTS tetrazolium compound was added to each well and 2.5 h later the absorbance at 490 nm was measured with a spectrofluorometer. Since all survival assays were done in triplicates, survival was calculated by normalizing the average absorbance of the samples to the absorbance of the untreated sample.

Viability of bacteria with and without added Au NPs was determined by counting colony forming units (CFU) on Luria broth agar plates. Bacterial cells (HI-PEMF and PEF treated and non-treated samples) were serially diluted with 0.9% NaCl and 100 μl of the dilution was plated into Luria broth agar medium (Sigma-Aldrich) with 50 μg/ml of kanamycin. Plates were then transferred in the incubator at 37 °C. After 24 h viability was determined as log (N/N0), where N represents the number of CFU/ml in treated sample and N0 the number of CFU/ml in untreated sample.

2.9. Electron microscopy

CHO cells and *E. coli* were centrifuged for 5 min at 200 g. Supernatant was discharged and fixative was added to cells. CHO cells were fixed in 4% formaldehyde plus 2% glutaraldehyde in 0.1 M sodium cacodylate buffer, pH 7.2, for 2 h and *E. coli* were fixed in 2.5% glutaraldehyde in 0.1 M sodium cacodylate buffer, pH 7.2 for 2.5 h. The following steps were the same for both cell types. Cells were centrifuged, fixative was removed and cells were washed in sodium cacodylate buffer and postfixed with 1% OsO_4 for 2 h. The samples were gradually dehydrated with ethanol and embedded in Epon. Ultrathin sections (50 nm thick) were cut, collected on carbon coated grids and stained with 2% uranyl acetate and Reynold's lead citrate. The sections were examined in Philips 100CM transmission electron microscope at 80 kV. Number of nanoparticles was estimated from the electron microscopy images using ImageJ software (National institutes of Health, Bethesda, MD, USA).

2.10. Statistical analysis

One-way analysis of variance (ANOVA; $p < 0.05$) was used to compare different treatments. Tukey's HSD multiple comparison test for evaluation of the difference was used when ANOVA indicated a statistically significant result ($p < 0.05$ was considered statistically significant).

3. Results

3.1. Distributed nanoelectrodes for local enhancement of electric field

Zeta-potential and number of Au NPs per μm^2 in two different buffers (citrate and PBS) at maximum used concentration (50 μg/ml) is shown in Table 1. Detailed characterization of nanoparticles is available in Supplementary Material (see Fig. S1 for TEM images of Au NPs and S2 for zeta-potential versus pH dependence).

According to theoretical and numerical predictions, local enhancement of electric field is possible when the conductive NPs are in close proximity with the plasma membrane [29,34,36]. Transmission electron microscopy (Fig. 2) confirmed that Au NPs are associated to the plasma membrane and outer membrane of the cell wall of CHO and *E. coli*, respectively, suggesting a potential local enhancement of electric field.

3.2. Au NPs enhanced HI-PEMF induced CHO permeabilization

The effect of HI-PEMF on permeabilization of CHO cells with and without Au NPs was analyzed. The representative shifts of fluorescence spectra for both PI and YP assays are shown in Fig. 3.

As it can be seen in Fig. 3, without NPs a minor shift due to HI-PEMF was detectable only in the YP assay (Fig. 3C). Whereas with Au NPs (20 nm, 50 μg/ml) the shift of spectra using the PI assay is more obvious compared to YP. The post-processed and normalized results of HI-PEMF induced electroporation separately and with NPs are shown in Fig. 4.

The HI-PEMF induced plasma membrane permeabilization without NPs was significantly increased ($p < 0.05$) only using the YP assay when the normalized median fluorescence was analyzed (Fig. 4B, D). With added Au NPs, HI-PEMF induced permeabilization was significantly increased in cells with added NPs of both sizes (5 or 20 nm). In general, permeabilization was dependent on the incubation time and was more efficient when 20 nm NPs were added (up to 80% permeabilization, Fig. 4C).

Plasma membrane permeabilization induced by HI-PEMF with added Au NPs has been also confirmed using fluorescence microscopy using PI assay. The number of fluorescent cells in untreated control (Fig. 5E) or HI-PEMF only (Fig. 5F) or samples with Au NPs only (Fig. G) was below 7 ± 3%. The HI-PEMF treatment with 20 nm Au NPs showed up to 49 ± 10% of PI permeabilized cells (Fig. 5H). In addition, bright field images of HI-PEMF treatment showed that the addition of Au NPs caused CHO cells to shrink (Fig. 5C, D).

The HI-PEMF treatment has no effect on survival of cells with added or without the Au NPs. There is no statistical difference between HI-PEMF treated (100% of survived cells) and untreated samples (97.4 ± 3.4% survived cells). Also, size or buffer of Au NPs do not influence cell survival, neither does incubation time (data not shown).

For comparison, permeabilization and survival of CHO cells exposed to PEF treatment with and without Au NPs was also ana-

Table 1
Number of 5 and 20 nm Au NPs in two different buffers incubated with CHO cells and *E. coli*.

Buffer	Size (nm)	Zeta-potential (mV)	NPs with CHO (N/μm^2)	NPs with *E. coli* (N/μm^2)
Citrate	5	−26.0 ± 0.5	20.8	/
	20	−18 ± 3	3.7	0.04
PBS	20	−17 ± 2	5.3	/

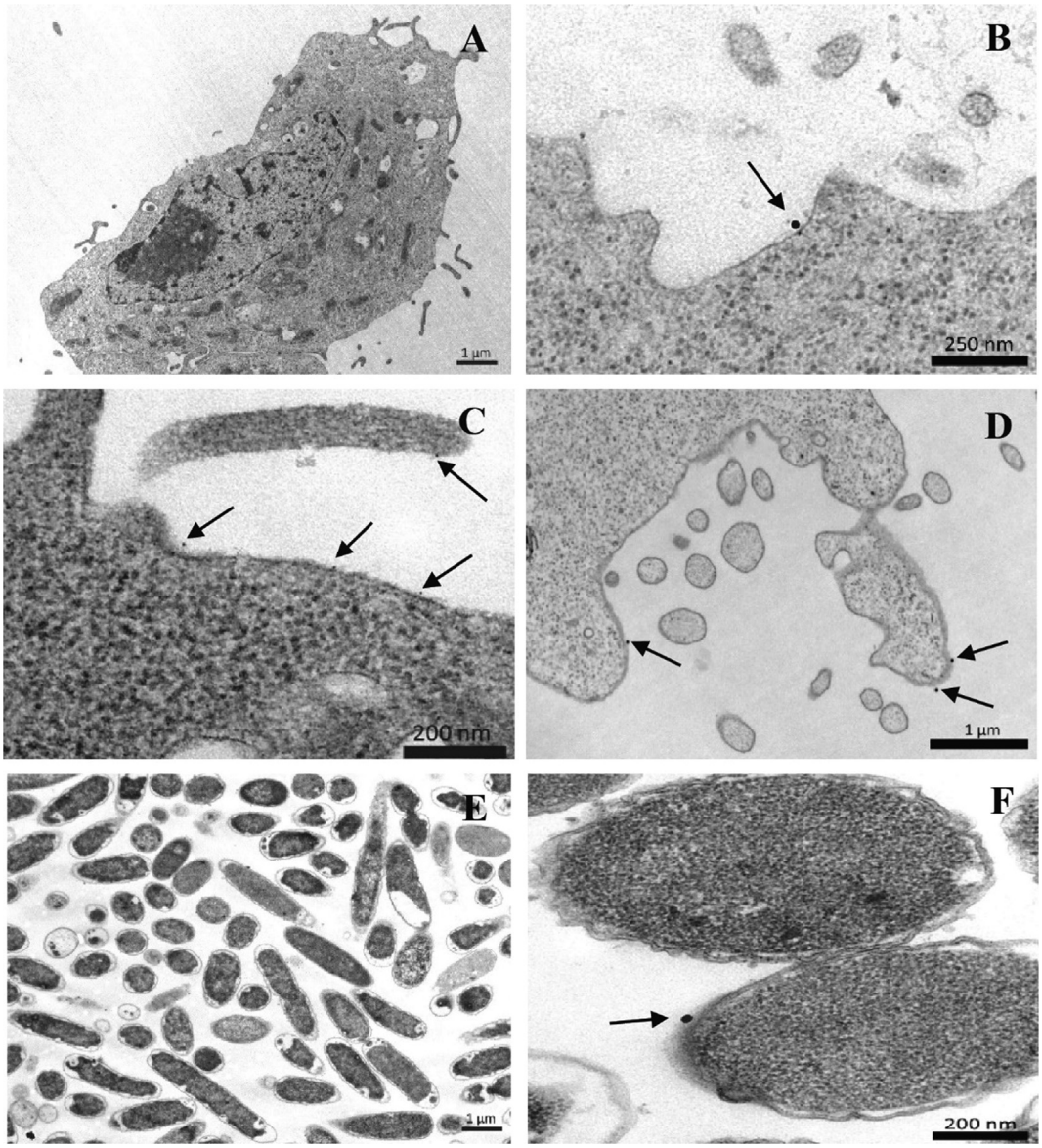

Fig. 2. Electron microscopy images of Au NPs (marked with black arrows) associated with the CHO plasma membrane and the outer membrane of the cell wall of *E. coli*, where A – CHO cells without Au NPs; B – CHO cells +20 nm Au NPs (citrate buffer); C – CHO cells +5 nm Au NPs (citrate buffer); D – CHO cells +20 nm Au NPs (PBS); E – *E. coli* without Au NPs; F – *E. coli* +20 nm Au NPs (citrate buffer).

lyzed. In general, fluorescence intensity of PI and YP was higher compared to HI-PEMF results, which is expected due to considerably higher electric fields of PEF.

In contrast to HI-PEMF treatment, survival of CHO cells exposed to PEF treatment was dependent on the size and the concentrations of Au NPs. Detailed results are available in Supplementary Material (see Figs. S4–5 and S6 for dependence of fluorescence intensity spectra and of survival on the applied electric field, respectively).

3.3. Au NPs enhanced HI-PEMF induced E. coli permeabilization

The same treatment methodology as with CHO cells was applied also for *E. coli*. HI-PEMF treatment also caused higher permeabilization of bacteria with added Au NPs in comparison to bacteria without Au NPs, but this was statistically significant only with 20 nm NPs (Table 2). HI-PEMF treatment had however no effect on survival of bacteria in the absence or presence of 20 nm Au NPs.

For comparison, treatment with PEF that employs more than 1500 times higher electric field compared to HI-PEMF, permeabilization of *E. coli* bacteria was higher and statistically significant difference was observed with Au NPs and without Au NPs, as well as between different sizes of Au NPs. Also, there was a difference in viability of *E. coli* bacteria after treatment with PEF without added Au NPs and with added 20 nm Au NPs.

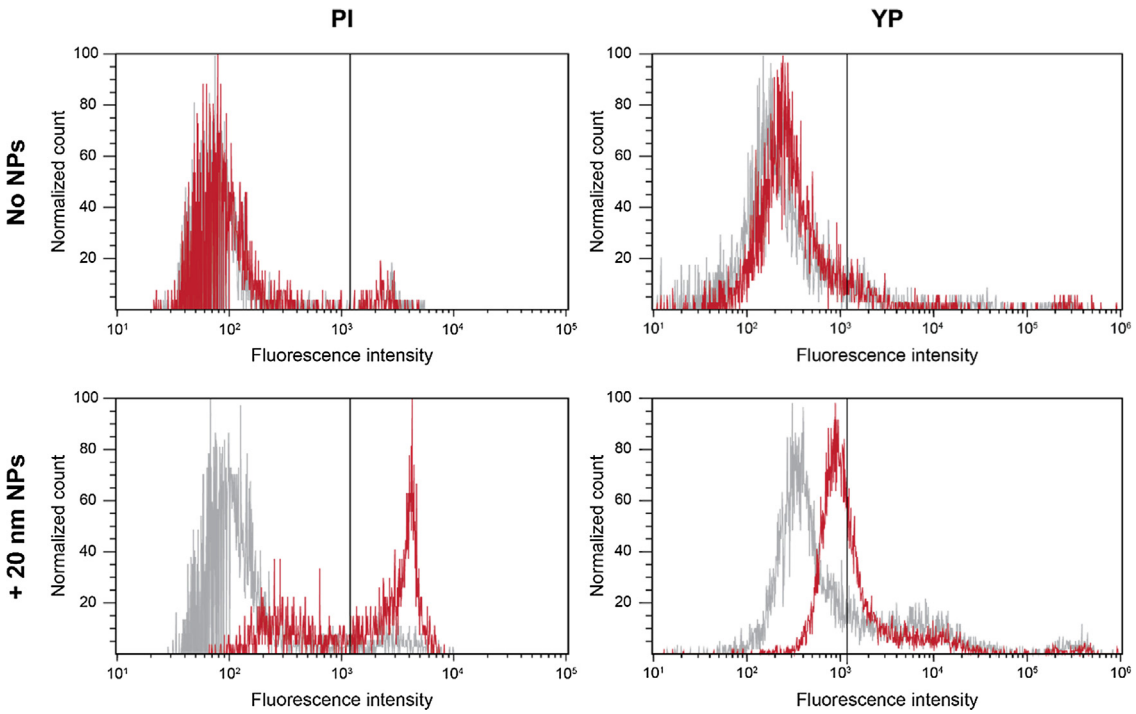

Fig. 3. The dependence of PI and YP fluorescence intensity spectra on HI-PEMF treatment samples without (grey plot) or with added 20 nm Au NPs (red plot). Left of the gate (black solid line) are non-permeabilized cells while right of the gate are permeabilized cells.

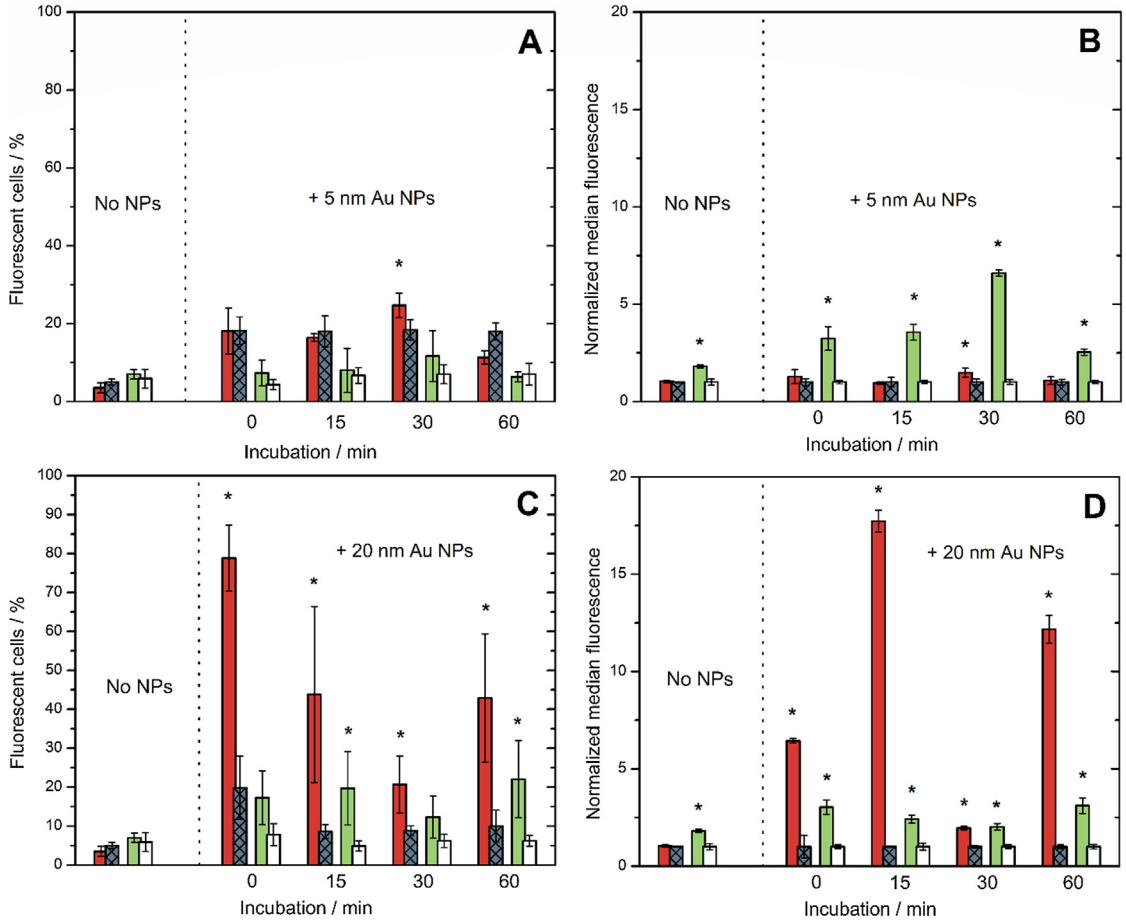

Fig. 4. Permeabilization of cells after HI-PEMF treatment. Cells without added NPs (No NPs) and cell with added 5 nm or 20 nm Au NPs (+5 or +20 nm Au NPs) were used. The percentage of PI (red) and YP (green) fluorescent cells (A, C) as well as median fluorescence (B, D) after different incubation time are shown. Each sample and fluorescent dye have their own untreated sample; CTRL PI (blue) or CTRL YP (white). Asterisk (*) marks statistically significant difference ($p < 0.05$) between treated sample and its corresponding untreated sample.

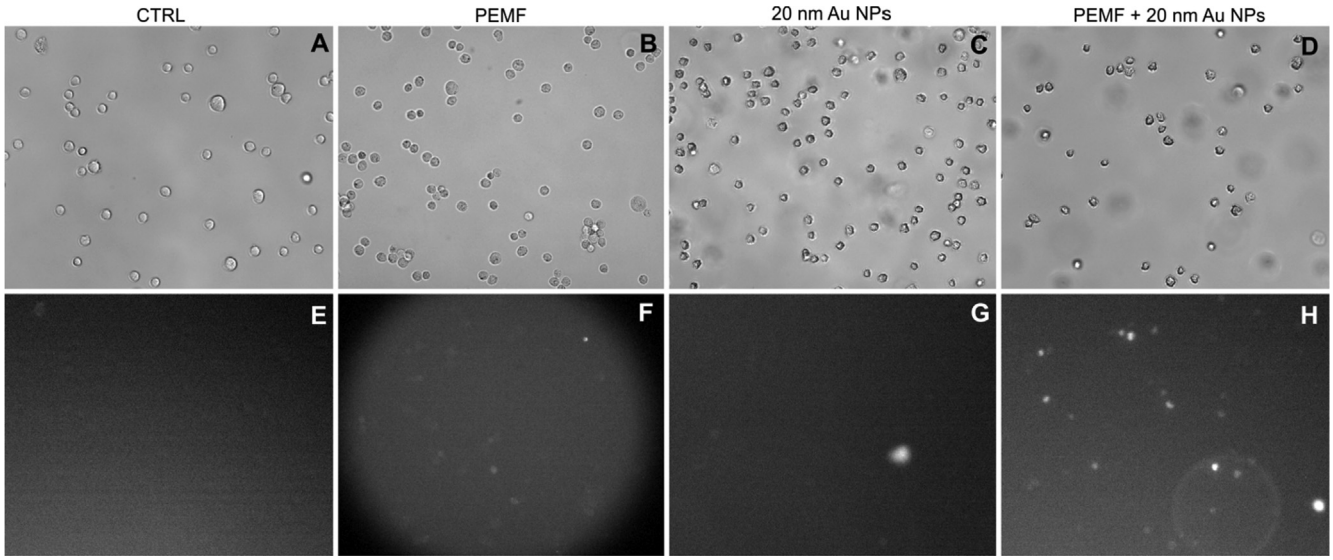

Fig. 5. Bright filed (A–D) and fluorescence microscopy images (E–H) of permeabilization after HI-PEMF was applied in PI assay. HI-PEMF untreated sample without added NPs (A, E), HI-PEMF treated sample without added NPs (B, F), HI-PEMF untreated sample with added NPs (C, G) and HI-PEMF treated sample with added NPs (D, H).

Table 2
Permeabilization and viability of *E. coli* after HI-PEMF treatment with 5 and 20 nm Au NPs (50 μg/ml). Permeabilization (mean ± standard deviation) was assessed by PI assay using spectrofluorometer, while viability was determined as log (N/N0), where N represents the number of CFU/ml in treated sample and N0 the number of CFU/ml in untreated sample. (*) represents statistically significant difference ($p < 0.05$). Each data point was repeated 3 times.

	PEMF (8 V/cm)		PEF (13 kV/cm)	
Size (nm)	Permeabilization (%)	Viability/logN/N0	Permeabilization (%)	Viability/logN/N0
No NPs	1.57 ± 0.7	−0.103	52.19 ± 10	−0.357
5	4.99 ± 2.3	/	81.53 ± 53 (*)	/
20	10.99 ± 4.0 (*)	−0.125	95.00 ± 5 (*)	−1.401

4. Discussion

Addition of nanoparticles during Pulsed Electric Fields (PEF) treatment allows modification of the extracellular medium conductivity and permittivity, while agglomeration of NPs near the membrane acts as distributed nanoelectrodes that locally enhance electric field and increase induced transmembrane voltage [29,30,34,36]. The proof of concept was confirmed both *in silico* [29,35] and *in vitro* [34–36], though only using PEF. In our study, we evaluated the feasibility to combine distributed nanoelectrodes in the form of Au NPs with High Intensity Pulsed Electromagnetic Fields (HI-PEMF) treatment for enabling higher efficacy of contactless membrane permeabilization. The speculations on the HI-PEMF induced permeabilization mechanism were always straightforwardly associated with electroporation due to linear dependence of the induced electric field on the *dB/dt* of the pulse [37,38]. Our data further support this hypothesis of electrostatics behind the formation of pores (we observe an increase of permeabilization presumably due to local field enhancement by Au NPs), however it does not explain the occurrence of permeabilization in fields that are by several orders lower when compared to conventional electroporation with PEF. High permeabilization (>80%) of CHO cells was achieved in PEF >400 V/cm (when enhanced by 20 nm Au NPs), however same levels of permeabilization were detected when the HI-PEMF induced electric field was merely 8 V/cm. Still, the number of applied electric pulses in PEF treatment was 8, which is considerably lower than 200 pulses applied in PEMF treatment. Observed discrepancy suggests to a relation between amplitude and number of pulses that results in the same level of permeabilization, similar as with conventional electroporation [39]. The HI-PEMF induced permeabilization was observed even in gram-negative bacteria, with more than 1500 times lower electric field compared to PEF, which further highlights the difference between the HI-PEMF and PEF. Significantly lower permeabilization thresholds for HI-PEMF could be associated with the hydrostatic pressure that is induced by the high time-varying magnetic fields, affecting the stretch-activated gating of ion channels and potentially pore opening and closing events [40–42]. Additionally, magnetically driven motion of ions may be responsible for the additional formation and concentration of surface charge on the membrane, which coupled with membrane deformation, enhance the permeabilization of the cell. Another possible mechanism is lipid oxidation which is achieved at lower electric fields than needed for electroporation, *i.e.*, pore formation [4,43]. However, the voltage controlled pore formation mechanism is still in place and the requirement of induced electric field to trigger the permeabilization process is absolute. This conclusion is in agreement with available experimental works [18–20,28,37,44,45], and establishes a high *dB/dt* as requirement for the HI-PEMF systems.

In our work, high permeabilization of CHO cells, which was enhanced by Au NPs depended on the size and concentration of NPs, but also incubation time. Smaller NPs internalize easier into the cells [46] and a smaller fraction may remain at the membrane than for the larger NPs despite the fact that, for the same concentration, there was a larger number of smaller particles. Nevertheless, the larger Au NPs (20 nm) used in this study show higher effect than the smaller ones (5 nm). Still, the results featured high deviations, which could be attributed to stability and size variation of NPs; the hydrodynamic sizes of the larger (20 nm) Au NPs were 36 and 30 nm for Au NPs in citrate and PBS buffer, respectively. The

larger hydrodynamic size with respect to the nominal size of the NPs originates from the electrostatic double layer at the surfaces of NPs dispersed in aqueous media. The later was confirmed with the high absolute zeta-potential values (Fig. S2). The polydispersity index (related to the hydrodynamic size) of 0.22 for both samples suggests on the narrow particle size distribution and good stability of the suspensions. On the other hand, the measurements of the 5 nm sized Au NPs were not reproducible. The obtained values ranged between 43 and 98 nm, which indicated on the poor stability of this particular suspension and particle agglomeration. Consequently, one of the reasons for the poorer efficiency of 5 nm Au NPs with respect to 20 nm Au NPs might also be attributed to their agglomeration or, as already mentioned, also easier internalization into the cells, leaving smaller fraction of NPs at the membrane.

The non-straightforward dependence of the pulsed electromagnetic fields induced permeabilization on the treatment parameters requires further research of different parameters of applied electromagnetic field. Moreover, the non-homogeneity of the induced electric field by HI-PEMF is a technological concern, which is typical to solenoid type inductor structures [18,38] and may also be the cause of the high standard deviation of data. Lastly, the non-controlled HI-PEMF induced dielectrophoretic movement of cells can also affect the treatment [47] and unequal exposure of different cells to HI-PEMF. The problem could be solved by the development of specific cuvettes for HI-PEMF *in vitro* work, which would allow physically restricting the placement of cells only in the high field region. Lastly, taking into account the contactless nature of the HI-PEMF technology and high potential of application in electroporation field-dominated areas, the improvement should also cover the generators development. Improvement of pulse generation through developing new magnetic pulse applicators, use of elongated nanoparticles or carbon nanotubes [29,31,48], further investigation of nanoparticles with attached ligands that selectively target specific cell sites [49–51], may result in a novel contactless delivery method that open up an avenue of possibilities for combining naked as well as functionalized Au NPs with HI-PEMFs for noninvasive, remotely controlled smart drug delivery applications.

5. Conclusion

Our results indicate that conductive gold nanoparticles can significantly potentiate the permeabilizing effect of HI-PEMF. This was shown on CHO cells and gram-negative bacteria with no effect on survival. Permeabilization efficacy was dependent on incubation time and on the size as larger nanoparticles had higher effect on permeabilization than the smaller ones. Future studies will focused on establishing a numerical model for in-depth analysis of nanoparticles placed in time-varying electromagnetic fields and for the investigation of interactions of nanoparticles with adjacent cell membranes.

Disclosure

Funding: This work was supported by the Slovenian Research Agency (research core funding No. P2-0249, P3-0108 and IP-0510, project No. J2-9225 to DM, funding for Junior Researcher to TP, and P2-0089 to DL). This work was also partly supported by the Research Council of Lithuania (Grant Nr. S-MIP-19-13). Experiments were performed within Infrastructure Programme: Network of research infrastructure centers at University of Ljubljana (MRIC UL IP-0510). Centers of Excellence NAMASTE, and Nanotechnology and Nanosciences are acknowledged for the usage of Zeta meter and TEM, respectively. The funders had no role in study design, data collection and analysis, decision to publish, or preparation of the manuscript. Authors declare no conflict of interest.

CRediT authorship contribution statement

Damijan Miklavcic: Conceptualization, Methodology, Resources, Supervision, Project administration, Funding acquisition, Writing - original draft. **Vitalij Novickij:** Conceptualization, Methodology, Investigation, Visualization, Formal analysis, Software, Writing - original draft. **Matej Kranjc:** Methodology, Investigation, Formal analysis, Visualization, Writing - review & editing, Writing - original draft, Software. **Tamara Polajzer:** Methodology, Investigation, Writing - original draf. **Sasa Haberl Meglic:** Methodology, Investigation, Writing - original draf. **Tina Batista Napotnik:** Methodology, Investigation, Writing - original draf. **Rok Romih:** Methodology, Investigation, Resources, Writing - original draf. **Darja Lisjak:** Methodology, Investigation, Resources, Writing - original draf.

Declaration of Competing Interest

The authors declare that they have no known competing financial interests or personal relationships that could have appeared to influence the work reported in this paper.

Appendix A. Supplementary material

Supplementary data to this article can be found online at https://doi.org/10.1016/j.bioelechem.2019.107440.

References

[1] T.Y. Tsong, Electroporation of cell membranes, Biophys. J. 60 (2) (1991) 297–306.
[2] J. Teissié, M.P. Rols, An experimental evaluation of the critical potential difference inducing cell membrane electropermeabilization, Biophys. J. 65 (1) (1993) 409–413.
[3] L. Rems, D. Miklavčič, Tutorial: electroporation of cells in complex materials and tissue, J. Appl. Phys. 119 (20) (2016) 201101.
[4] T. Kotnik, L. Rems, M. Tarek, D. Miklavčič, Membrane electroporation and electropermeabilization: mechanisms and models, Annu. Rev. Biophys. 48 (1) (2019) 63–91.
[5] T. Batista Napotnik, M. Reberšek, P.T. Vernier, B. Mali, D. Miklavčič, Effects of high voltage nanosecond electric pulses on eukaryotic cells (in vitro): a systematic review, Bioelectrochemistry 110 (2016) 1–12.
[6] A. Polak et al., Electroporation of archaeal lipid membranes using MD simulations, Bioelectrochemistry 100 (2014) 18–26.
[7] T. Kotnik, W. Frey, M. Sack, S. Haberl Meglič, M. Peterka, D. Miklavčič, Electroporation-based applications in biotechnology, Trends Biotechnol. 33 (8) (2015) 480–488.
[8] D.L. Perrier, L. Rems, P.E. Boukany, Lipid vesicles in pulsed electric fields: Fundamental principles of the membrane response and its biomedical applications, Adv. Colloid Interface Sci. 249 (2017) 248–271.
[9] T. García-Sánchez, R. Bragós, L.M. Mir, In vitro analysis of various cell lines responses to electroporative electric pulses by means of electrical impedance spectroscopy, Biosens. Bioelectron. 117 (2018) 207–216.
[10] L. Liu, Z. Mao, J. Zhang, N. Liu, Q.H. Liu, The influence of vesicle shape and medium conductivity on possible electrofusion under a pulsed electric field, PLoS ONE 11 (7) (2016) e0158739.
[11] A. Peyman et al., Variation in dielectric properties due to pathological changes in human liver, Bioelectromagnetics 36 (8) (2015) 603–612.
[12] L.G. Campana et al., Electrical resistance of human soft tissue sarcomas: an ex vivo study on surgical specimens, Med. Biol. Eng. Compu. 54 (5) (2016) 773–787.
[13] G. Pataro, M. Falcone, G. Donsì, G. Ferrari, Metal release from stainless steel electrodes of a PEF treatment chamber: effects of electrical parameters and food composition, Innov. Food Sci. Emerg. Technol. 21 (2014) 58–65.
[14] F. Maglietti, S. Michinski, N. Olaiz, M. Castro, C. Suárez, G. Marshall, The role of Ph fronts in tissue electroporation based treatments, PLoS One 8 (11) (2013) e80167.
[15] E. Luján, M. Marino, N. Olaiz, G. Marshall, Towards an optimal dose-response relationship in gene electrotransfer protocols, Electrochim. Acta 319 (2019) 1002–1011.
[16] E. Guenther, N. Klein, P. Mikus, M.K. Stehling, B. Rubinsky, Electrical breakdown in tissue electroporation, Biochem. Biophys. Res. Commun. 467 (4) (2015) 736–741.

[17] L. Rubinsky, E. Guenther, P. Mikus, M. Stehling, B. Rubinsky, Electrolytic effects during tissue ablation by electroporation, Technol. Cancer Res. Treat. 15 (5) (2016), NP95–NP103.
[18] V. Novickij, J. Dermol, A. Grainys, M. Kranjc, D. Miklavčič, Membrane permeabilization of mammalian cells using bursts of high magnetic field pulses, PeerJ 5 (April) (2017).
[19] S. Kranjc, M. Kranjc, J. Scancar, J. Jelenc, G. Sersa, D. Miklavcic, Electrochemotherapy by pulsed electromagnetic field treatment (PEMF) in mouse melanoma B16F10 in vivo, Radiol. Oncol. 50 (1) (2016) 39–48.
[20] V. Novickij, A. Grainys, I. Kucinskaite-Kodze, A. Zvirbliene, J. Novickij, Magneto-permeabilization of viable cell membrane using high pulsed magnetic field, IEEE Trans. Magn. 51 (9) (2015) 1–5.
[21] D.C. Sweeney, M. Reberšek, J. Dermol, L. Rems, D. Miklavčič, R.V. Davalos, Quantification of cell membrane permeability induced by monopolar and high-frequency bipolar bursts of electrical pulses, Biochim. Biophys. Acta – Biomembr. 1858 (11) (2016) 2689–2698.
[22] J. Dermol, D. Miklavčič, Mathematical models describing chinese hamster ovary cell death due to electroporation in vitro, J. Membr. Biol. 248 (5) (2015) 865–881.
[23] V. Novickij et al., Measurement of transient permeability of Sp2/0 myeloma cells: flow cytometric study, Meas. Sci. Rev. 16 (6) (2016) 300–304.
[24] M.B. Sano, C.B. Arena, M.R. DeWitt, D. Saur, R.V. Davalos, In-vitro bipolar nano- and microsecond electro-pulse bursts for irreversible electroporation therapies, Bioelectrochemistry 100 (2014) 69–79.
[25] M. Kranjc, S. Kranjc, F. Bajd, G. Serša, I. Serša, D. Miklavčič, Predicting irreversible electroporation-induced tissue damage by means of magnetic resonance electrical impedance tomography, Sci. Rep. 7 (1) (2017) 10323.
[26] M.B. Sano, R.E. Fan, L. Xing, Asymmetric waveforms decrease lethal thresholds in high frequency irreversible electroporation therapies, Sci. Rep. 7 (2017).
[27] C. Jiang, R.V. Davalos, J.C. Bischof, A review of basic to clinical studies of irreversible electroporation therapy, IEEE Trans. Biomed. Eng. 62 (1) (2015) 4–20.
[28] V. Novickij et al., Pulsed electromagnetic field assisted in vitro electroporation: a pilot study, Sci. Rep. 6 (1) (2016) 33537.
[29] J. Lekner, Electroporation in cancer therapy without insertion of electrodes, Phys. Med. Biol. 59 (20) (2014) 6031–6042.
[30] H. Qiu, R.P. Joshi, A. Pradhan, Simulation of nanoparticle based enhancement of cellular electroporation for biomedical applications, J. Appl. Phys. 116 (18) (2014).
[31] G. Bocharov, A. Eletskii, Theory of carbon nanotube (CNT)-based electron field emitters, Nanomaterials 3 (3) (2013) 393–442.
[32] V. Raffa, C. Riggio, M.W. Smith, K.C. Jordan, W. Cao, A. Cuschieri, BNNT-mediated irreversible electroporation: its potential on cancer cells, Technol. Cancer Res. Treat. 11 (5) (2012) 459–465, https://doi.org/10.7785/tcrt.2012.500258.
[33] Z. Rezaee, A. Yadollahpour, V. Bayati, F.N. Dehbashi, Gold nanoparticles and electroporation impose both separate and synergistic radiosensitizing effects in HT-29 tumor cells: an in vitro study, Int. J. Nanomedicine 12 (2017) 1431–1439.
[34] Y. Zu, S. Huang, W.C. Liao, Y. Lu, S. Wang, Gold nanoparticles enhanced electroporation for mammalian cell transfection, J. Biomed. Nanotechnol. 10 (6) (2014) 982–992.
[35] S. Huang, Y. Zu, S. Wang, Gold nanoparticle-enhanced electroporation for leukemia cell transfection, Methods Mol. Biol. 1121 (2014) 69–77.
[36] A. Ghorbel, L.M. Mir, T. García-Sánchez, Conductive nanoparticles improve cell electropermeabilization, Nanotechnology 30 (49) (2019) 495101.
[37] T.J. Kardos, D.P. Rabussay, Contactless magneto-permeabilization for intracellular plasmid DNA delivery in-vivo, Hum. Vaccin. Immunother. 8 (11) (2012) 1707–1713.
[38] A. Lucinskis, V. Novickij, A. Grainys, J. Novickij, S. Tolvaisiene, Modelling the cell transmembrane potential dependence on the structure of the pulsed magnetic field coils, Elektron. ir Elektrotechnika 20 (8) (2014) 9–12.
[39] G. Pucihar, J. Krmelj, M. Rebersek, T. Napotnik, D. Miklavcic, Equivalent pulse parameters for electroporation, IEEE Trans. Biomed. Eng. 58 (11) (2011) 3279–3288.
[40] T. Polyakova, V. Zablotskii, A. Dejneka, Cell membrane pore formation and change in ion channel activity in high-gradient magnetic fields, IEEE Magn. Lett. 8 (2017).
[41] Vitalii Zablotskii, Tatyana Polyakova, Oleg Lunov, Alexandr Dejneka, How a high-gradient magnetic field could affect cell life, Sci. Rep. 6 (1) (2016), https://doi.org/10.1038/srep37407.
[42] V. Zablotskii, O. Lunov, S. Kubinova, T. Polyakova, E. Sykova, A. Dejneka, Effects of high-gradient magnetic fields on living cell machinery, J. Phys. D Appl. Phys. 49 (49) (2016) 493003, https://doi.org/10.1088/0022-3727/49/49/493003.
[43] K.A. Runas, N. Malmstadt, Low levels of lipid oxidation radically increase the passive permeability of lipid bilayers, Soft Matter 11 (3) (2015) 499–505.
[44] Z. Shankayi, S.M.P. Firoozabadi, M. Mansourian, A. Mahna, The effects of pulsed magnetic field exposure on the permeability of leukemia cancer cells, Electromagn. Biol. Med. 33 (2) (2014) 154–158.
[45] L. Towhidi, S.M.P. Firoozabadi, H. Mozdarani, D. Miklavcic, Lucifer Yellow uptake by CHO cells exposed to magnetic and electric pulses, Radiol. Oncol. 46 (2) (2012) 119–125.
[46] K. Huang et al., Size-dependent localization and penetration of ultrasmall gold nanoparticles in cancer cells, multicellular spheroids, and tumors in vivo, ACS Nano 6 (5) (2012) 4483–4493.
[47] V. Novickij, A. Grainys, J. Novickij, Contactless dielectrophoretic manipulation of biological cells using pulsed magnetic fields, IET Nanobiotechnol. 8 (2) (2014) 118–122.
[48] V. Raffa, G. Ciofani, O. Vittorio, V. Pensabene, A. Cuschieri, Carbon nanotube-enhanced cell electropermeabilisation, Bioelectrochemistry 79 (1) (2010) 136–141.
[49] E. Wagner, D. Curiel, M. Cotten, Delivery of drugs, proteins and genes into cells using transferrin as a ligand for receptor-mediated endocytosis, Adv. Drug Deliv. Rev. 14 (1) (1994) 113–135.
[50] K.R. Colacino, C.B. Arena, S. Dong, M. Roman, R.V. Davalos, Y.W. Lee, Folate conjugated cellulose nanocrystals potentiate irreversible electroporation-induced cytotoxicity for the selective treatment of cancer cells, Technol. Cancer Res. Treat. Abril (16) (2014) 1–10.
[51] P. Tiwari, K. Vig, V. Dennis, S. Singh, Functionalized gold nanoparticles and their biomedical applications, Nanomaterials 1 (1) (2011) 31–63.